

Detecting early response to therapy in liver cancer treatment: 3D metastases segmentation using graph-cuts with a modified prior

Tünde Szilágyi^{a*}, Michael Verhoek^a and J. Alison Noble^a

^aEngineering Science Department, University of Oxford, Oxford, UK

Abstract. Accurate 3D liver metastasis extraction is one of the most important steps in treatment planning for patients with advanced colorectal cancer. In this paper we present a semi-automatic segmentation algorithm based on graph cuts theory with a prior which uses both intensity values and local phase information. The segmentation method is tested on images from three patients and the new results are compared to manual segmentations and previously proposed methods. A Dice coefficient accuracy of 83-92% is achieved. Advantages of this semi-automated method over existing RECIST estimations include non-subjective volume assessment over time for patients undergoing treatment and minimal user interaction.

1 Introduction

Monitoring the response of tumours to treatment is of vital importance for cancer patients undergoing therapy. There is no defined protocol. Therapy assessment criteria that have been considered include physiological measurements and imaging, and one way of using the latter is to quantify volume changes. Tumour volumes are calculated based on uni- and bidimensional manual measurements following the guidelines established by the World Health Organization and more recently the Response Evaluation Criteria in Solid Tumours, known as the RECIST criteria [1]. However, these measurements are subjective, time consuming and provide inaccurate volume estimations [2]. These points and the fact that hepatic tumour delineation has high inter- and intra observer variability ($> 8\%$) are the main driving force behind automatic segmentation methodology development.

Automatic and semi-automatic segmentation algorithms are challenging to develop because a high diversity of tumour masses arise with varying shape and homogeneity. The boundaries of the tissue of the organ and tumour are not well separated, especially in the case of hepatic metastases, due to the mixing of the tumour rim and normal liver parenchyma.

In this paper we explored graph-cuts for the segmentation of hepatic metastases. Prior attempts to use this technique were limited due to the restricted structural information included in the intensity based prior. We address this limitation by defining a prior not only by pixel intensity values but also by local phase and adaptive anisotropic diffusion of the local phase maps. Local phase carries important structural information that is invariant to local intensity variations. This paper first presents the methodology including graph cuts, modified prior, and the proposed algorithm. Then we report on results applied to 3D (stacks of 2D slices) contrast-enhanced CT abdominal images from patients with advanced colorectal cancer (CRC).

2 Methods

Segmentation of liver metastases from advanced CRC patients was performed using a semi automated graph-cuts segmentation algorithm. Familiarity with graph theory terminology is assumed, otherwise the reader is referred to [3].

2.1 Experimental Data and Images

Patients with hepatic metastases from advanced CRC considered for this study underwent chemotherapy in regular three months cycles, followed by an assessment of the response by imaging. Disease progression was evaluated by looking at the changes in lesion volume using contrast enhanced CT images and physiology measurements of specific tumour markers, such as CA-19. Prior to the imaging examination, patients received Gastrografin and Niopam 300 contrast agent intravenously (IV). CT images were collected using a LightSpeed Ultra spiral CT scanner at the Churchill Hospital, Oxford with a slice thickness of 5 mm and an in-plane resolution of $0.97\text{ mm} \times 0.97\text{ mm}$, each of 512×512 pixels.

*Corresponding author: Tünde Szilágyi: tuende.szilagyi@eng.ox.ac.uk. Tünde Szilágyi is supported by the Engineering and Physical Research Council of the UK through a Life Science Interface Doctoral Training Centre Studentship (grant reference EP/E501605/1). Michael Verhoek is sponsored by a Microsoft Research studentship.

2.2 The Algorithm: 3D segmentation using graph-cuts with a modified prior

Our semi-automated segmentation algorithm uses graph cuts theory and assumes that the liver was identified prior to this. The schematic of the algorithm is shown in Figure 1.

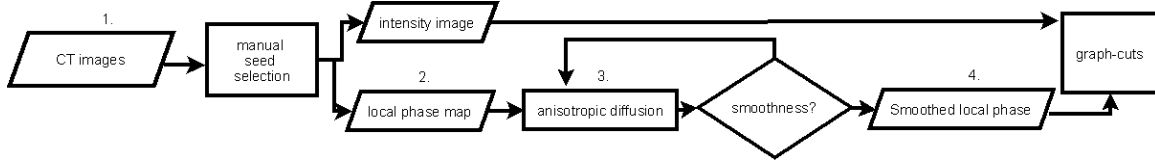


Figure 1. The Algorithm. 1. the seed points for the background and foreground are selected using a user interface; 2. Local phase is computed; 3. local phase is smoothed adaptively given the homogeneity of the region measured by the variance of the object seed; 4. both the initial intensity map, the smoothed local phase map; the likelihood function and boundary term eq. (4) are passed on to the Graph Cuts algorithm.

Within the graph-cuts framework a stack of images of dimension $M \times N \times K$ is represented by a graph $\mathcal{G} = (\mathcal{V} \cup \{s, t\}, \mathcal{E})$ with $(M \times N \times K) + 2$ vertices, where \mathcal{V} contains the image pixel, $\{s, t\}$ are the terminal nodes (source and sink respectively) for binary segmentation tasks, and \mathcal{E} contains the weighted edges. For the remainder of this paper n-links denote the connecting edges between neighbouring voxels, when a neighbourhood \mathcal{N} can have arbitrary shape and extension, and t-links the edges between voxels and terminal nodes. The process of segmentation is then achieved by finding the minimum cost cut that separates s and t and which corresponds to the data driven global energy minimization. Consider the generalized energy function [4], $E(x_1, \dots, x_n) = \sum_i E^i(x_i) + \sum_{i < j} E^{ij}(x_i, x_j)$, where E is a function of n binary valued variables. The regularity or submodularity condition shows that E is graph representable iff each term satisfies the condition: $E^{i,j}(0, 0) + E^{i,j}(1, 1) \leq E^{i,j}(0, 1) + E^{i,j}(1, 0)$. Then the posterior probability of the segmentation S given an input image X becomes [4] $p(S | X) \propto e^{-E}$, where E for segmentation purposes is represented by a region coherence (R) and boundary term (B) as:

$$E(A) = \lambda \cdot R(A) + B(A) \quad (1)$$

Here A is a binary labelling and λ controls the relative importance of R and B . R is a negative log likelihood function, based on interactive selection of seed points in the foreground (\mathcal{F}) and background (\mathcal{B})

$$R_p(A_p = \text{foreground}) = -\ln(P(I_p | \mathcal{F})), \quad (2)$$

$$R_p(A_p = \text{background}) = -\ln(P(I_p | \mathcal{B})). \quad (3)$$

I_p denotes the intensity value or another measure associated with pixel p (i.e. local phase [5]).

Finally, B is a modified Ising prior [6]

$$B = \sum_{p, q \in \mathcal{N}} \left(|A_p - A_q| e^{-\left(\frac{\|I_p - I_q\|^2}{2\sigma^2}\right)} - \kappa \cdot e^{-\left(\frac{\|LP_p - LP_q\|^2}{2\sigma^2}\right)} \right) \frac{1}{\|p - q\|}, \quad (4)$$

where LP denotes the local phase and κ controls the relative importance of the intensity and local phase terms, and σ is a factor describing the noise due to camera optics (the blur). In our experiments we used $\kappa = 0.34$ and a 6-neighbourhood. Local phase (LP) was derived from the monogenic signal [5] signal using the Mellor-Brady filter [7] as: $LP = \tan^{-1} \left(\frac{b}{\sqrt{r_1^2 + r_2^2}} \right)$, where b denotes the bandpass signal, and r_1 and r_2 are respectively the Riesz transform pairs (Figure 4). Unwanted local phase variability within anatomical regions, here liver, was removed using anisotropic diffusion and parameters described next.

Anisotropic diffusion was applied to local phase maps as described in [8]. The parameters used here are as follows: an integration constant $\delta = \frac{1}{7}$, conduction control term (i.e. gradient modulus) $\kappa = 30$, conduction coefficient function as for wide regions as proposed in the original work [8].

Accuracy of the segmentation was estimated by $\frac{M_1 - M_2}{\sigma_1 \cdot \sigma_2}$, where M_1 and M_2 are the mean values of the intensity based histograms derived from the seeds from the liver parenchyma and tumour respectively, and σ_1 and σ_2 are the corresponding variances.

Ground truth metastases and liver mask segmentations were carried out manually (by the first author, a non specialist) using a pen tab device (Cintiq company) and ITK-SNAP 1.6.0.1.

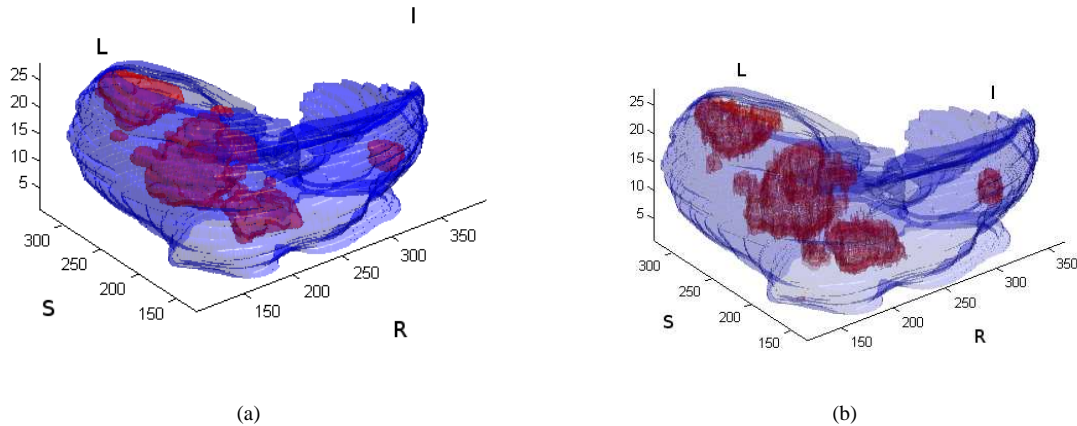


Figure 2. 3D visualisation of the liver metastases from Patient 2. Note the difference in the smoothness of the metastases surfaces. This is a result of the fact that manual segmentations usually avoid capturing the fine details of the edges. A λ value of 450 was used. S denotes superior, I inferior, R right and L left position of the patient. (a) Both the metastases (red, small ball like structures) and the liver (blue, encompassing geometry) are a result of manual segmentation. (b) Metastases segmented using the proposed method. The surface of the segmented metastases were not smoothed or adjusted with the λ parameter - this results in a hairy appearance of the rendered metastases.

Validation of the results was performed by comparing to manual segmentation using the Dice Similarity Coefficient (DSC) [9] and to previously reported results using the volumetric overlap and relative absolute volume difference. These measures are defined in Table 1.

Measure	DSC	$V_{overlap}$	D_{rel}
Definition	$\frac{2 \#(S_1 \cap S_2)}{\#S_1 + \#S_2}$	$\frac{\#(S_1 \cap S_2)}{\#(S_1 \cup S_2)}$	$\frac{\#S_1}{\#S_2} - 1$

Table 1. Definition of the measures used to compute segmentation accuracy. # denotes the cardinality of sets, S_1 is the segmentation achieved by the proposed algorithm and S_2 is the "ground truth" from manual segmentation. Full overlap results in a DSC and volumetric overlap of 1 and relative absolute difference of 0.

3 Results and Discussion

Three patients' data were segmented using the new methodology one of which had multiple (three) timepoint data during treatment. 3D rendering of the segmentation results from the algorithm and manual segmentation is presented in Figure 2(b) and Figure 2(a), while an example of 2D segmentation results is shown in Figure 4. Here, the segmented metastases show a less smooth appearance compared to the manual segmentation. This results from the underlying mixture of normal and cancerous tissue explained in the introduction and which would be too onerous to take into account when performing manual segmentation. This smoothness can be partly controlled by the λ parameter.

The relative importance of the region and boundary terms was examined by varying the parameter λ and the results are presented in Figure 3(a). This test confirmed that the range of optimal λ parameters was identified as 450 – 500, and which does not change for different patients, given the same imaging modality and protocol.

Accuracy was assessed for different patients and the same patient at changing timepoints using the criteria presented in Table 1. This is summarized in Table 2 and 3. Table 2 shows that an accuracy of 83.8-91.5 % DSC, 72.32-83.4% volumetric overlap and 0.0198-0.2134 % relative difference error is achieved for the analyzed data. These results are superior to the ones presented for the MICCAI Liver Tumour Segmentation Competition 2008 ($V_{overlap}$): max. 46.64 % in [10], max. 51.40 % [11], max 50.52 % [12]. We note here that results from the MICCAI 2008 were obtained for the data sets selected for the competition, whereas our images were taken from a specific CRC study. We argue that the significantly better performance of our method is due to the fact that previous methods relied on intensity only, whereas we included local phase in our knowledge based prior, which is a good quantifier of structural information.

The accuracy achieved by our methodology for the metastases segmentation is reasonable given that liver metastases

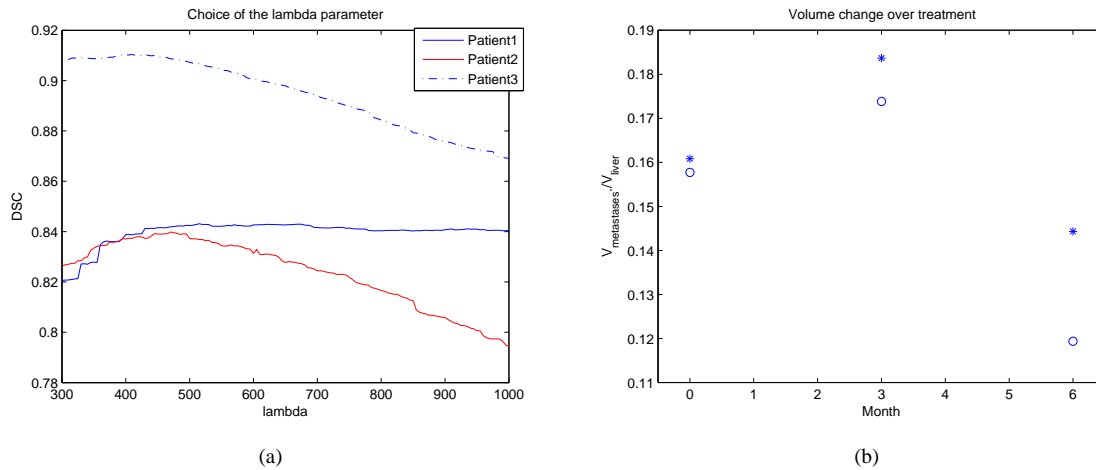


Figure 3. (a) The impact of the relative terms in the energy function (i.e. boundary and region terms) controlled by the lambda parameter. Note that the optimal value for this parameter is within the same range 450-500 for all the images used. (b) Change of volume over a six month time period. Note the initial increase in the tumour volume and then shrinking at the end of the sixth month. Additionally, notice the increasing difference between the manual (circles) and metastases segmented using the proposed algorithm (asterisk). This is the result of the increased "fuzzy" appearance of the tumours due to therapy. A lambda value of 480 was used.

from CRC have a papillary structure which means that at the rim of the tumour both invasive tumour cells and normal tissue cells are present. Therefore manual segmentation of large tumour masses is not obvious and usually the segmentations do not follow the exact structure of the metastases rim.

Our aim was to propose a method that could be used for volume estimations of CRC liver metastases as a possible way to assess therapy effectiveness. This requires objective assessment of tumour masses during treatment. Figure 3(b) shows that the difference between the proposed segmentation and the manual segmentation increases during therapy, which is also reflected in the accuracy measure presented in Table 3, and is a result of the increased inhomogeneity and less defined edges of the tumour. Additionally, note that initially the volume of the metastases is increasing and therefore metastases volume might not be the best indicator of therapy effectiveness; instead, a joint model based on volumetric changes and a tumour rim descriptor might be considered.

Patient id / Criteria	Patient 1	Patient 2	Patient 3
DSC %	84.22	83.93	91.5
$V_{overlap}$ %	72.74	72.32	83.4
D_{rel} %	1.85	1.69	1.98
accuracy $\times 10^{-4}$	12	2.39	0.405

Table 2. Segmentation accuracy measures for Patient 1, Patient 2 and Patient 3. The details of the calculations are given Table 1.

Patient 3 / Criteria	0th month	3rd month	6th month
DSC %	91.5	90.21	86.87
$V_{overlap}$ %	83.40	82.16	76.78
D_{rel} %	1.98	5.66	20.91
accuracy $\times 10^{-3}$	4.05	0.9865	0.9028

Table 3. Segmentation accuracy differences influenced by the changes in the tumour appearance during treatment.

4 Conclusion

We explored the application of graph-cuts to liver metastases segmentation with priors based on intensity and local phase measures. This method proved to be computationally time efficient and achieved a good accuracy with respect to manual segmentation, with DSC values of 83-92 %. The presented tool could be an integral part of the decision making when fused together with other tools such as liver segmentation and hepatic vasculature segmentation [13]. Finally, our volume estimation results should be validated on larger data sets, and additional measurements made that capture the changes which appear at the rim of the tumour during therapy.

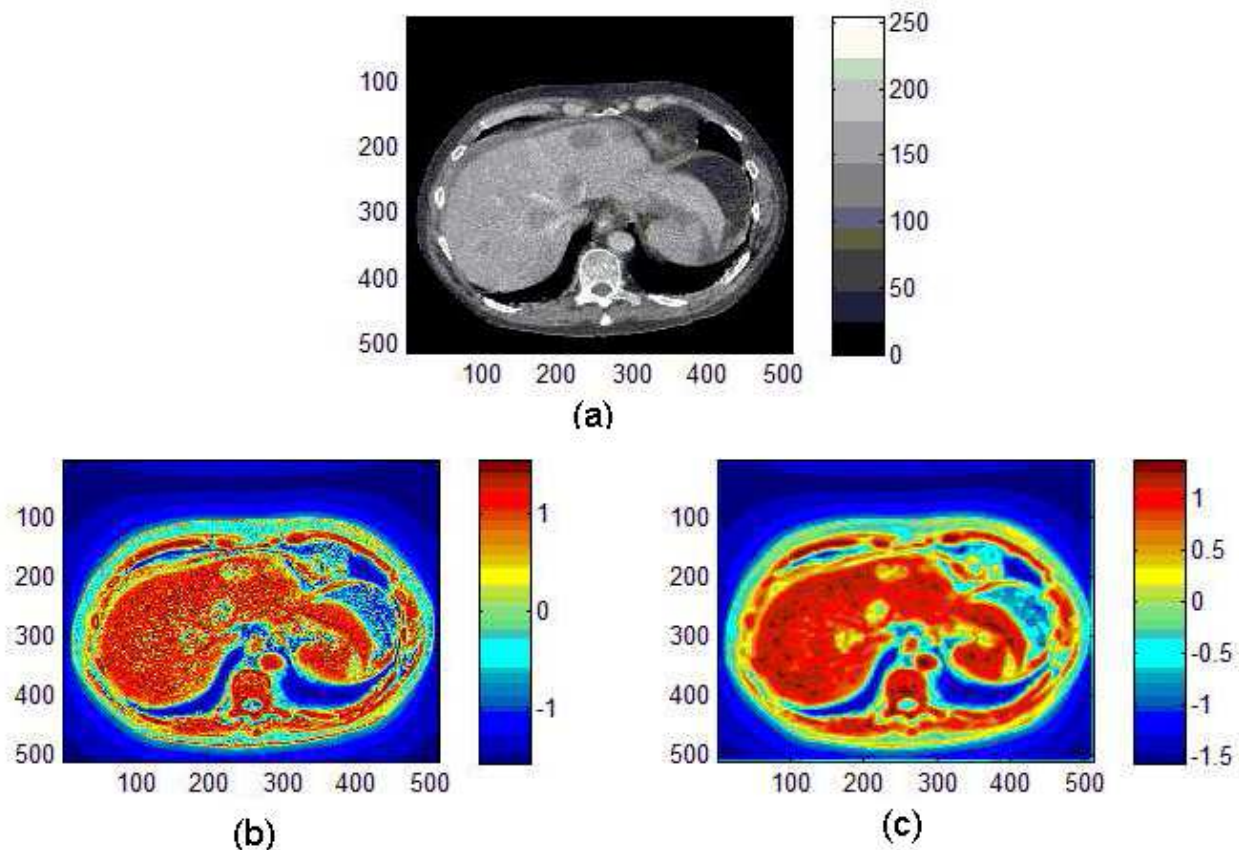


Figure 4. Smoothed local phase information. (a) Original 8 bit contrast enhanced CT image. (b) Local phase map from a single scale, empirically selected. (c) Local phase smoothed with anisotropic diffusion - for parameters refer to the text. Note the difference in smoothness in the appearance between (b) and (c).

Acknowledgment

The authors would like to thank Professor David Kerr, Dr. Yoko Yanagisawa and Dr. Mark Anderson for their continued assistance throughout this project.

References

1. P. Therasse, S. G. Arbutk, E. A. Eisenhauer et al. "New guidelines to evaluate the response to treatment in solid tumors." *J Nat Cancer Inst* **92**, pp. 205–216, 2000.
2. S. R. Prasad, K. Jhaveri, S. Saini et al. "Ct tumour measurements for therapeutic response assessment: Comparison of unidimensional, bidimensional, and volumetric techniques - initial observations." *Radiology* **225**, pp. 416–419, 2002.
3. N. Paragios, Y. Chen & O. Faugeras. *Handbook of Mathematical Models in Computer Vision*. Springer.
4. V. Kolmogorov & R. Zabih. "What energy functions can be minimized via graph-cuts." *IEEE PAMI* **26**, pp. 147–159, 2004.
5. M. Felsberg & G. Sommer. "The monogenic signal." *IEEE Trans. on Signal Proc.* **49**, pp. 3136–3144, 2001.
6. Y. Boykov & M.-P. Jolly. "Interactive graph cuts for optimal boundary and region segmentation of objects in n-d images." *ICCV* 2001.
7. M. Mellor & M. Brady. "Non-rigid multimodal image registration using local phase." *MICCAI* 2004.
8. P. Perona & J. Malik. "Scale-space and edge detection using anisotropic diffusion." *IEEE PAMI* **12**, pp. 629–639, 1990.
9. L. R. Dice. "Measures of the amount of ecologic association between species." *Ecology* **26**, pp. 297–302, 1945.
10. J. H. Moltz, L. Bornemann, V. Dicken et al. "Segmentation of liver metastases in ct scans by adaptive thresholding and morphological processing." *MICCAI* 2008.
11. Y. Haeme. "Liver tumour segmentation using implicit surface evolution." *MICCAI* 2008.
12. D. Smeets, B. Stijnen, D. Loeckx et al. "Segmentation of liver metastases using a level set method with spiral-scanning technique and supervised fuzzy pixel classification." *MICCAI* 2008.
13. H. Homann, G. Vesom & J. A. Noble. "Vasculature segmentation of ct liver images using graph cuts and graph-based analysis." *5th IEEE Int. Symp on Biomedical Imaging* 2008.